

Tunable Directional Filter for Mid-Infrared Optical Transmission Switching

ANDREW BUTLER, JACK SCHULZ, AND CHRISTOS ARGYROPOULOS*

Department of Electrical and Computer Engineering, University of Nebraska-Lincoln, Lincoln, Nebraska 68588, USA

**christos.argyropoulos@unl.edu*

Abstract: Controlling the spectral and angular response of infrared (IR) radiation is a challenging task of paramount importance to various emerging photonic applications. Here, we overcome these problems by proposing and analyzing a new design of a tunable narrowband directional optical transmission filter. The presented thermally controlled multilayer filter leverages the temperature dependent phase change properties of vanadium dioxide (VO_2) to enable efficient and reversible fast optical switching by using a pump-probe laser excitation setup. More specifically, transmission is blocked for high intensity probe lasers due to the VO_2 metallic properties induced at elevated temperatures while at low probe laser intensities high transmission through the filter occurs only for a narrowband IR range confined to near normal incident angles. The proposed multilayer composite dielectric filter is expected to have applications in optical communications, where it can act as dual functional infrared filter and optical switch.

1. Introduction

Recently, the emerging area of tunable photonics has attracted increased attention as an efficient way to design new optical devices that can dynamically adapt their properties to a variety of diverse applications. A particular phase change material commonly used in tunable photonic applications is vanadium dioxide (VO_2). It undergoes a reversible phase transition from insulator to metal as its temperature is increased by switching phases at a critical temperature ($\sim 340\text{K}$) [1], which can be controlled and tuned via doping with tungsten [2]. Thus, VO_2 enables efficient thermal control over the optical properties of photonic structures that is incorporated into. Many works were focused on using VO_2 to thermally switch between states of high and low reflection, transmission, or absorption. As an example, tunable reflection in the visible spectrum was demonstrated by using VO_2 as a defect layer in a Bragg filter design [3]. Enhanced tunability of absorption/emissivity in the mid-infrared (IR) band was demonstrated using a multilayer design composed of alternating layers of VO_2 and metals [4]. Another design utilized the refractive index change of VO_2 to create a tunable optical response in a thin film structure [5]. A VO_2 filled double cavity was designed for operation in the near IR that could act as band-pass filter or optical switch [6]. More recently, switchable transmission in the mid-IR range was demonstrated using a thin VO_2 layer in a multilayer filter design [7]. However, most of the previously works demonstrate switching and reconfigurability only by varying the bulk temperature of the obtained device and not by dynamically changing the incident laser power in a pump-probe laser experimental configuration setup. The latter approach will be much faster in terms of switching operation since laser-induced heating can occur in extremely fast time scales [8].

Another important aspect of light propagation that the works above do not consider is filtering the incident angle of light that can be narrowed to a small range leading to directional transmission response. For full control of light, it is desirable for optical filters to not only control the spectral response but also the spatial directionality of incident light. In the past, angular filtering of light was demonstrated using a multilayer structure surrounded by a fluid

serving as broadband impedance matching to the surrounding material [9]. This multilayer filter design featured efficient and broadband transmission restricted to only angles near 60° , however the design only worked for transverse-magnetic (TM) polarized light which limits its thermal emission applications. A narrowband polarization independent filter that confines the transmission of light to only near normal incidence has also been demonstrated in recent years [10]. While both of these designs perform well in terms of simultaneous spectral and angular filtering, they have no mechanisms to control or modulate their behavior which will be very beneficial for tunable photonic filter applications.

As mentioned before, another interesting application for tunable filters is optical switching based on pump-probe laser experiments. The binary switching of VO_2 between two phases makes it a good candidate for use in various switching scenarios. Optical switching using VO_2 thin films [11,12] and fast switching using VO_2 nanocrystals has been demonstrated for operation at near-IR frequencies [13]. Other designs have attempted to improve the modulation depth in the near-IR range, such as structures consisting of gold nanowires over a VO_2 thin spacer layer that leverages the plasmonic modes of metallic VO_2 to enhance tunability [14]. In the mid-IR range, another design used a two-dimensional (2D) array of aluminum nanoantennas over a thin VO_2 layer that alternated between high reflection and absorption depending on the VO_2 phase [15]. However, both these works require complex nanostructuring which makes their fabrication challenging and impractical.

Beyond VO_2 , several alternative methods exist to create tunable filters and optical switches. Graphene is one common approach, where the Fermi energy of graphene can be tuned via electrostatic gating. This allows for control over the plasmonic resonances of graphene enabling tunable optical filters consisting of graphene layers combined with plasmonic gratings [16,17]. However, the use of graphene can result in additional fabrication complexity. Other techniques to create optical switches include controlling the position of liquid droplets [18], or the use of liquid crystals [19], Dirac semimetals [20], and topological semimetals based on antimonene [21]. A notable advantage of VO_2 over the other approaches is that the extreme difference between its metallic and insulating phase enable very high modulation depths [15] that can occur in rapid time scales in case the phase transition is induced by probe lasers.

In this work, we present the design of a new optically switchable narrowband directional transmission filter based on a simple multilayer dielectric structure. We utilize the thermally dependent optical properties of VO_2 to introduce control in the directional filtering response. When the VO_2 layers are in the insulating phase, the structure exhibits very narrowband transmission of light at incident angles close to normal. In the metallic phase, the VO_2 layers prevent transmission through the structure and turn the device to a mirror or absorber of mid-IR radiation when high probe laser intensities are utilized. The optical response of the design is accurately analyzed using the transfer matrix method and the dynamic temperature dependence is characterized using the VO_2 Bruggeman effective medium theory. Transient modeling under pump-probe laser illumination is carried out to demonstrate the applicability of the presented filter to fast optical switching at the mid-IR range. The presented directional and rapid switching response is unique among other relevant optical filters and provides an additional degree of control compared to other designs. The proposed optical filter is envisioned to have a plethora of photonic applications, such as infrared filtering and optical switching.

2. Narrowband directional filter analysis

The schematic of the proposed multilayer directional transmission filter is shown in Fig. 1a. The design consists of five unit cells of alternating layers of VO_2 and calcium fluoride (CaF_2). The thickness of each VO_2 layer is 450nm while each CaF_2 layer is $2.55\mu\text{m}$ thick. Both VO_2 and CaF_2 materials are modelled using their frequency dispersive dielectric constants obtained from relevant experimental data [22–24]. In the insulating state, the VO_2 acts as a high refractive index dielectric. When combined with the low index CaF_2 material, a special Bragg mirror effect occurs that works for both polarizations, creating a band of high reflection at

wavelengths above $7.7\mu\text{m}$. At the edge of this reflection band, a transmission resonance occurs, and a highly directional response is obtained. In a typical Bragg reflector design, the layer thicknesses are chosen to be $\frac{1}{4}$ the center wavelength of the stop band. Using this as a starting point, the thicknesses of the layers were optimized until the highly narrowband directional transmission results were obtained. The multilayer structure can be feasibly fabricated using thin film deposition techniques. Growth of VO_2 thin films on the order of 100nm thick have been demonstrated using RF magnetron sputtering [25] and thicker high quality VO_2 films have recently been demonstrated using the vapor transport method [26]. Likewise, CaF_2 films of micron thickness have been deposited using resistive evaporation [27]. Alternating these deposition techniques can realize the filter's multilayer structure.

The computed transmittance versus wavelength is shown in Fig. 1b at the primary resonance of the structure. The full width at half maximum (FWHM) for this resonance is found to be $\sim 240\text{nm}$ which further demonstrates that the presented response is very narrowband. The transmittance spectra as a function of incidence angles are shown in Fig. 1c for TM polarization and Fig. 1d for transverse-electric (TE) polarization when VO_2 is in the insulating phase. A broader wavelength range is shown that includes multiple higher order resonances. These results prove that the presented filter can work for both polarizations, i.e., incoherent light illumination, consisting ideal property for thermal imaging and sensing. In the metallic VO_2 phase, the transmission is zero for all wavelengths and incident angles and the filter exhibits mirror-like response for near-normal incidence, while higher angles of incidence show broadband absorption. More information on the reflectance and absorptance in the metallic state is available in the Supplementary Information [28]. Figure 1e demonstrates the directional response of the filter when VO_2 is in the insulating phase, where it is confirmed that the optical transmission is limited to only a small range of angles near normal incidence. Interestingly, the narrowband directional response is maintained for a reduced number of material layers without a drastic drop in performance, as discussed in more details at the Supplementary Information [28].

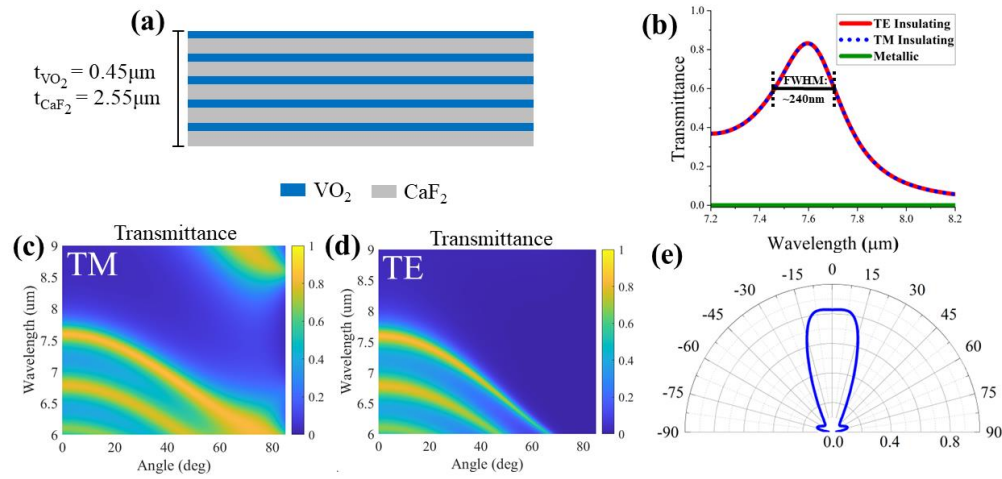


Fig 1. (a) Schematic of the multilayer directional transmission filter. (b) Transmittance as a function of wavelength for normal incidence illumination. Only the primary resonance is shown. There is substantial transmission change between insulating and metallic VO_2 phases. (c)-(d) Transmittance as a function of wavelength and incident angle for (c) TM and (d) TE polarization. A broader wavelength range containing higher order resonances is shown in these figures. (e) Directional transmittance pattern as a function of angle for fixed $7.6\mu\text{m}$ operation wavelength.

The transmittance spectra shown in Figs. 1b-e were obtained analytically using the transfer matrix method. Each layer was modelled as a transmission line and the ABCD parameters for each layer were obtained using [29]:

$$\begin{bmatrix} A & B \\ C & D \end{bmatrix} = \begin{bmatrix} \cos(kt) & jZ \sin(kt) \\ j\frac{1}{Z} \sin(kt) & \cos(kt) \end{bmatrix}, \quad (1)$$

where t is the thickness of the layer, $k = k_0 \sqrt{\varepsilon - \sin^2(\theta)}$ is the wavevector in the material, and $Z = \eta_0 / \sqrt{\varepsilon - \sin^2(\theta)}$ is the impedance for TE polarization, while the impedance becomes $Z = \eta_0 \sqrt{\varepsilon - \sin^2(\theta)}$ for TM polarization. The impedance of free space is η_0 (377Ω), $k_0 = 2\pi / \lambda$, ε is the complex frequency dependent dielectric constant of each material, and θ is the incident angle. The total ABCD matrix for the whole multilayer structure can be obtained by multiplying the ABCD matrices of each layer:

$$\begin{bmatrix} A & B \\ C & D \end{bmatrix}_{tot} = \begin{bmatrix} A & B \\ C & D \end{bmatrix}_1 \begin{bmatrix} A & B \\ C & D \end{bmatrix}_2 \cdots \begin{bmatrix} A & B \\ C & D \end{bmatrix}_{10}. \quad (2)$$

The transmission coefficient (S_{21}) through the structure can be found by converting the ABCD parameters of Eq. (2) into the S-parameters [29]:

$$S_{21} = \frac{2}{A + \frac{B}{Z_0} + CZ_0 + D}, \quad (3)$$

where the free space impedance for oblique incident waves is $Z_0 = \eta_0 / \cos(\theta)$ for TE polarization and $Z_0 = \eta_0 \cos(\theta)$ for TM polarization. The transmittance through the structure is then found as $|S_{21}|^2$.

From the results in Figs. 1b-e, it can be derived that the transmission through the filter is very narrowband at $\sim 7.6\mu\text{m}$ and is restricted to within $\sim 15^\circ$ from normal incidence. This small transmission band leads to narrow directional spatial filtering obtained at the edge of the multilayer structure's stopband. The highest transmission occurs closest to the stopband of the filter, though the fringes at lower IR wavelengths can also be used for similar performance filtering. The operating wavelength and fringe wavelengths can be adapted to different frequency ranges by simple redesigning the layer thicknesses. Interestingly, the presented filter design is polarization independent, thus the filter can be used with randomly polarized incoherent light sources, e.g., mid-IR thermal emission.

The directionality was further verified using finite element method 2D full wave simulations. An out of plane line current was used to model a point source located above the filter at a wavelength of $7.6\mu\text{m}$. Again, the VO_2 and CaF_2 materials were modeled using their frequency dependent dielectric constants [22–24]. The induced field distributions through the filter for the VO_2 insulating and metallic phases are shown in Figs. 2a and 2b, respectively. Directional radiation is only present for the VO_2 insulating phase (Figs. 2a) while the transmission is terminated when the VO_2 is metallic (Figs. 2b). These results further prove the unique directionality and tunability of the filter design.

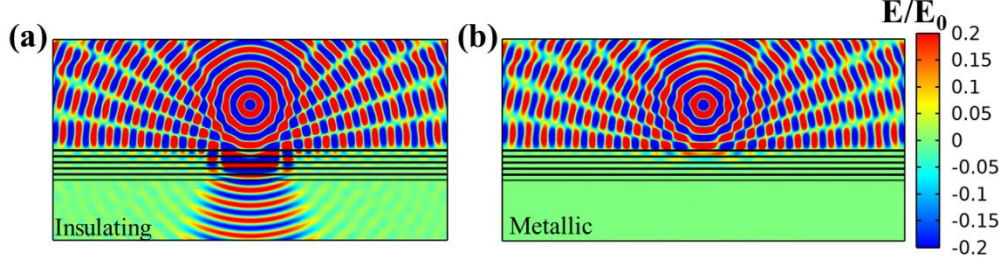


Fig 2: Field distributions through the presented directional filter using a point source when VO₂ is in the (a) insulating and (b) metallic phase, respectively.

The transmission of the presented filter does not change abruptly during the VO₂ phase transition process, but it has a dynamic temperature dependent response that follows the change of the VO₂ dielectric constant. More specifically, the VO₂ phase transition occurs at the critical temperature ($T_c \approx 340K$). Interestingly, the VO₂ phase is in transition mode at temperatures very close to critical, and its complex dielectric constant can be accurately computed by using the Bruggeman effective medium theory [30]:

$$\varepsilon_{VO_2} = \frac{1}{4} \left[\varepsilon_i(2-3V) + \varepsilon_m(3V-1) + \sqrt{[\varepsilon_i(2-3V) + \varepsilon_m(3V-1)]^2 + 8\varepsilon_i\varepsilon_m} \right], \quad (4)$$

where ε_m is the VO₂ dielectric constant in the metallic phase, ε_i is the dielectric constant in the insulating phase [24], and V is the metallic volume fraction that can be calculated by using the formula:

$$V = 1 - \frac{1}{1 + \exp\left(\frac{T - T_c}{\Delta T}\right)}, \quad (5)$$

where T is the ambient temperature, T_c is the VO₂ critical temperature, and $\Delta T=2K$ [29] is the transition width. The formulas in Eqs. (4)-(5) can be used in the calculations of Eqs. (1)-(3) to accurately compute the dynamic temperature response of the filter. The transmission dependence on the temperature for normal incidence illumination at the optimal wavelength of $7.6\mu m$ is demonstrated in Fig. 3a. In addition, the angular response of the transmittance is shown in Fig. 3b as a function of temperature again at the fixed wavelength of $7.6\mu m$.

The switching behavior of the optical filter as the temperature is increased is not abrupt but it has a dynamic transition range which is clearly illustrated in Fig. 3a. At lower temperatures than T_c , when VO₂ is in the insulating phase, transmission through the structure is greater than 80%, similar to Fig. 1b. At higher temperatures compared to T_c , VO₂ transitions to the metallic phase and transmission drops to zero. However, the directionality of the filter is maintained during the insulating and transition phases, as depicted in Fig. 3b. The relative abrupt but continuous transition between phases can enable fast optical transmission switching and modulation when the temperature rapidly changes. This type of response is ideal for efficient infrared optical communications, where the selective angular response of the filter can be used to eliminate noise and erroneous stray signals coming from oblique incident angles. Furthermore, the VO₂ critical temperature can be further reduced via doping with tungsten, thus the presented optical filter can be made tunable and even operate at room temperature.

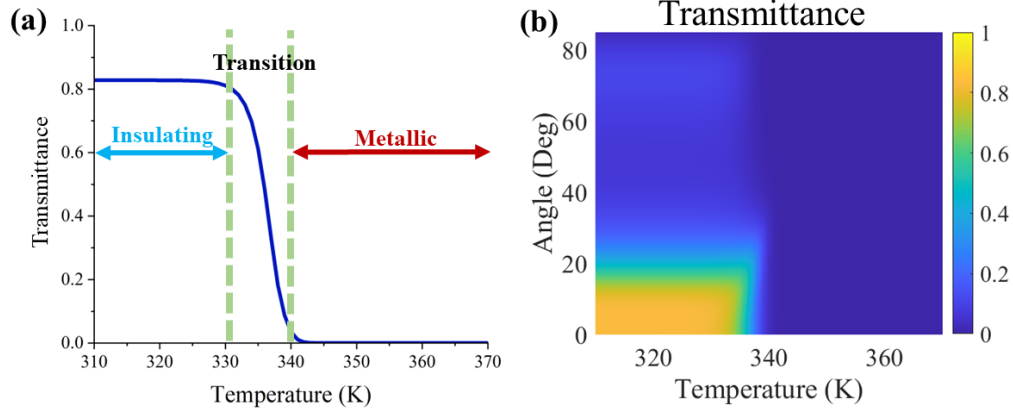


Fig 3. (a) Dynamic transmission response versus temperature at normal incidence illumination. The temperature ranges from insulating to metallic VO₂ phase and a clear transition area occurs before the VO₂ critical temperature T_c. (b) Angular transmittance as a function of temperature. Both results are plotted at a fixed wavelength of 7.6μm.

3. Optical transmission switching

Transient simulations based on pump-probe laser excitations are performed to demonstrate the ability of the directional filter to operate as a fast optical transmission switch. The heating process in the simulations is induced by the pump laser excitations, where two different lasers operating at distinct wavelengths and input intensities are used. A detailed explanation of the transient simulations is available in the Supplementary Information [28]. Comsol Multiphysics® is used to simulate the thermal and optical behavior of the filter. The pump and probe lasers are modelled as plane waves which are launched towards the multilayer structure. Although typical laser pulses have a gaussian beam spatial profile, their spatial extent usually covers a large area. Hence, we focus our simulations near the maximum of the spatial gaussian beam distribution and approximate the impinging lasers as plane waves. The temperature of the structure is initialized to room temperature (293K) and the Comsol's electromagnetic heating interface is used to determine the heating of the structure according to the following equations:

$$Q_e = Q_{rh} + Q_{ml}, \quad (6)$$

$$Q_{rh} = \frac{1}{2} Re(\mathbf{J} \cdot \mathbf{E}^*), \quad (7)$$

$$Q_{ml} = \frac{1}{2} Re(i\omega \mathbf{B} \cdot \mathbf{H}^*), \quad (8)$$

where Q_e is the total heat added to the system from electromagnetic heating, Q_{rh} is the heat from resistive losses, Q_{ml} is the heat from magnetic losses, \mathbf{J} is the current density, \mathbf{E} is the induced electric field, ω is the angular frequency, and \mathbf{B} and \mathbf{H} are the induced magnetic flux density and field, respectively. For each time step, the temperature of the filter is first determined using Eqs. (6-8) and then the optical constants of VO₂ are calculated using Eq. (4). The optical constants of VO₂ are then plugged into an electromagnetic simulation to determine the reflectance and transmittance of the filter. The probe laser is launched as a monochromatic plane wave and the power flow through the structure is measured. The calculated transmittance is then recorded for each time step. A simple schematic of the pump-probe simulation setup is shown in the inset of Fig. 4d.

The first choice of pump laser is a Thulium (Tm) doped fiber laser operating at a wavelength of 1940nm with intensities of 5, 7.5, and 10mW/cm² [31]. The second pump choice is an yttrium vanadate (Nd:YVO₄) laser operating at 532nm with slightly lower intensities of 2.5, 5, and 7.5mW/cm² [32]. The chosen pump lasers are commercially available continuous wave (CW) lasers, but their excitation is chosen to last for 5ms to allow the structure to cool

and demonstrate its transmission switching behavior during the different phases. The filter is always illuminated by a normal incident low power laser source acting as probe with fixed wavelength ($7.6\mu\text{m}$) in the mid-IR range that does not cause additional heating. The computed induced temperature along the filter as a function of time for the two pump lasers is demonstrated in Figs. 4a and 4b, respectively. The filter is initially held at room temperature (293K). Heating is practically uniform throughout the structure, and the computed temperature represents the average temperature through the entire filter geometry. The induced temperature exceeds the critical temperature (purple dashed line in Figs. 4a and 4b) associated to the VO_2 phase transition, as was described in Fig. 3. This phase transition leads to a transient and relatively abrupt switching in the transmittance of the filter for each probe laser which is depicted in Figs. 4c and 4d.

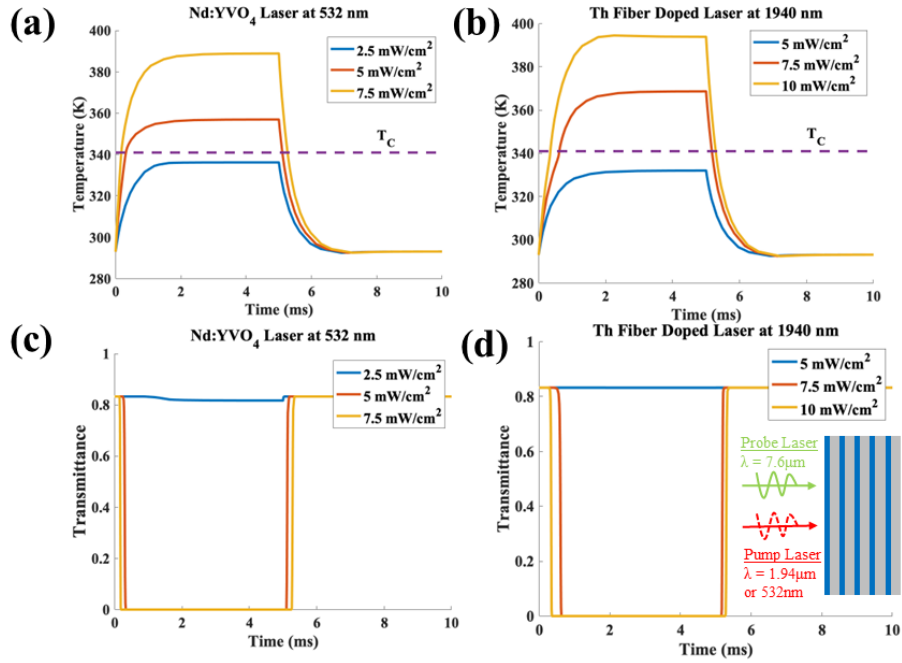


Fig 4. (a)-(b) Temperature and (c)-(d) transmittance of the directional filter as a function of time for the (a), (c) Nd:YVO₄ and (b), (d) Th doped fiber pump laser, respectively. The transient results are presented for different pump laser intensities. (Inset in (d)) A simple schematic of the simulation setup showing the pump/probe scheme.

The process of transmission switching takes less than a millisecond with both currently used pump lasers. More specifically, it is derived from Fig. 4 that the insulating to metallic phase change occurs at approximately 635 μs and 361 μs for the fiber laser at 7.5 and 10 mW/cm² intensities, respectively. The transition from the metallic back to the insulating state takes 240 μs and 368 μs for the same laser with similar intensities. In the case of the yttrium vanadate laser, the insulator-metal transition occurs at 335 μs and 186 μs while the metal-insulator transition happens at 176 μs and 335 μs for intensities of 5 and 7.5 mW/cm² respectively. We define the insulator-metal transition time as the time it takes for the transmission to drop to zero after the start of the pump laser pulse. The metal-insulator transition time is defined as the time it takes for the transmission to increase back to maximum after the pump laser pulse is removed. The yttrium vanadate laser has faster switching performance mainly due to the stronger absorption of insulating VO_2 in the visible emitting wavelength of this pump laser. The filter's switching process can become even faster, approaching few micro- or pico-seconds, if less layers (see Supplementary Information [28]) or ultrafast pulsed lasers are used, respectively, resulting to a more rapid heating process [33-35]. The results shown here are very fast compared to other

relevant schemes, such as liquid-based switching, which had a ~200ms response time [18], or liquid crystal designs that had switching times on the order of milliseconds [19].

4. Conclusions

We presented the design of a new thermally controlled directional narrowband optical transmission filter. The use of VO₂ enables tunable and fast switching response between high and zero transmission. The transmission through the filter is limited to narrow bands in the mid-IR range and only light near normal incidence is allowed to pass through the filter. The filter works for both polarizations and, as a result, can operate with incoherent light sources, such as thermal radiation. The proposed optical filter will have applications in infrared optical communications, where its switching capability and directional selective transmission can lead to a reconfigurable and tunable response [36].

Funding. This work was partially supported by the Office of Naval Research Young Investigator Program (ONR-YIP) (Grant No. N00014-19-1-2384), the National Science Foundation/EPSCoR RII Track-1: Emergent Quantum Materials and Technologies (EQUATE) (Grant No. OIA-2044049), and the NASA Nebraska Space Grant Fellowship.

References

1. B. Ko, T. Badloe, and J. Rho, "Vanadium Dioxide for Dynamically Tunable Photonics," *ChemNanoMat* 7(7), 713–727 (2021).
2. V. N. Andreev and V. A. Klimov, "Metal–Insulator Phase Transition in Tungsten-Doped Vanadium Dioxide Thin Films," *Physics of the Solid State* 2019 61:8 61(8), 1471–1474 (2019).
3. X. I. Wang, Z. Gong, K. Dong, S. Lou, J. Slack, A. Anders, and J. Yao, "Tunable Bragg filters with a phase transition material defect layer," *Optics Express*, Vol. 24, Issue 18, pp. 20365–20372 24(18), 20365–20372 (2016).
4. R. L. Voti, M. C. Larciprete, G. Leahu, C. Sibilia, and M. Bertolotti, "Optimization of thermochromic VO₂ based structures with tunable thermal emissivity," *J Appl Phys* 112(3), 034305 (2012).
5. D. de Ceglia, M. Grande, A. Vincenti, C. Baratto, and C. de Angelis, "Tunable filters for visible light based on resonant VO₂ planar thin films," *International Conference on Transparent Optical Networks* 2020-July, (2020).
6. D. Chauhan, Z. Sbeah, R. Adhikari, M. S. Thakur, S. H. Chang, and R. P. Dwivedi, "Theoretical analysis of VO₂ filled double rectangular cavity-based coupled resonators for plasmonic active switch/modulator and band pass filter applications," *Opt Mater (Amst)* 125, 112078 (2022).
7. C. Wan, D. Woolf, C. M. Hessel, J. Salman, Y. Xiao, C. Yao, A. Wright, J. M. Hensley, and M. A. Kats, "Switchable Induced-Transmission Filters Enabled by Vanadium Dioxide," *Nano Lett* 22(1), 6–13 (2022).
8. L. Khosravi Khorashad and C. Argyropoulos, "Unraveling the temperature dynamics and hot electron generation in tunable gap-plasmon metasurface absorbers," *Nanophotonics* 11(17), 4037–4052 (2022).
9. Y. Shen, D. Ye, I. Celanovic, S. G. Johnson, J. D. Joannopoulos, and M. Soljačić, "Optical Broadband Angular Selectivity," *Science* (1979) 343(6178), 1499–1501 (2014).
10. Q. Qian, C. Xu, and C. Wang, "All-dielectric polarization-independent optical angular filter," *Scientific Reports* 2017 7:1 7(1), 1–7 (2017).
11. M. Soltani, M. Chaker, E. Haddad, R. v. Kruzelecky, and D. Nikanpour, "Optical switching of vanadium dioxide thin films deposited by reactive pulsed laser deposition," *Journal of Vacuum Science & Technology A: Vacuum, Surfaces, and Films* 22(3), 859 (2004).
12. M. Soltani, M. Chaker, E. Haddad, and R. Kruzelesky, "1 × 2 optical switch devices based on semiconductor-to-metallic phase transition characteristics of VO₂ smart coatings," *Meas Sci Technol* 17(5), 1052 (2006).
13. A. Cavalleri, L. C. Feldman, L. A. Boatner, M. Rini, R. López, R. F. Haglund, R. W. Schoenlein, and T. E. Haynes, "Photoinduced phase transition in VO₂ nanocrystals: ultrafast control of surface-plasmon resonance," *Optics Letters*, Vol. 30, Issue 5, pp. 558–560 30(5), 558–560 (2005).
14. A. Ninawe, A. Dhawan, A. Thomas, K. Kumar, and P. Savaliya, "Au nanowire-VO₂ spacer-Au film based optical switches," *JOSA B*, Vol. 35, Issue 7, pp. 1687–1697 35(7), 1687–1697 (2018).
15. Q. Wang, S. Zhang, C. Wang, R. Li, T. Cai, and D. Zhang, "Tunable Infrared Optical Switch Based on Vanadium Dioxide," *Nanomaterials* 2021, Vol. 11, Page 2988 11(11), 2988 (2021).
16. A. Dubrovkin, B. Hu, J. Tao, Q. J. Wang, and X. Yu, "Graphene-based tunable plasmonic Bragg reflector with a broad bandwidth," *Optics Letters*, Vol. 39, Issue 2, pp. 271–274 39(2), 271–274 (2014).
17. Z. X. Jia, Y. Shuai, S. D. Xu, and H. P. Tan, "Graphene-Based Tunable Metamaterial Filter in Infrared Region," *Smart Science* 4(3), 127–133 (2016).
18. H. Ren, S. Xu, Y. Liu, and S. T. Wu, "Liquid-based infrared optical switch," *Appl Phys Lett* 101(4), 041104 (2012).

19. P. G. LoPresti, P. Zhou, R. G. Linquist, and I. C. Khoo, "All-Optical Switching of Infrared Optical Radiation Using Isotropic Liquid Crystal," *IEEE J Quantum Electron* 31(4), 723–728 (1995).
20. C. Zhu, F. Wang, Y. Meng, X. Yuan, F. Xiu, H. Luo, Y. Wang, J. Li, X. Lv, L. He, Y. Xu, J. Liu, C. Zhang, Y. Shi, R. Zhang, and S. Zhu, "A robust and tuneable mid-infrared optical switch enabled by bulk Dirac fermions," *Nature Communications* 2017 8:1 8(1), 1–7 (2017).
21. T. Hai, G. Xie, J. Ma, H. Shao, Z. Qiao, Z. Qin, Y. Sun, F. Wang, P. Yuan, J. Ma, and L. Qian, "Pushing Optical Switch into Deep Mid-Infrared Region: Band Theory, Characterization, and Performance of Topological Semimetal Antimonene," *ACS Nano* 15(4), 7430–7438 (2021).
22. W. Kaiser, W. G. Spitzer, R. H. Kaiser, and L. E. Howarth, "Infrared Properties of CaF_2 , SrF_2 , and BaF_2 ," *Physical Review* 127(6), 1950 (1962).
23. I. H. Malitson, "A Redetermination of Some Optical Properties of Calcium Fluoride," *Applied Optics*, Vol. 2, Issue 11, pp. 1103–1107 2(11), 1103–1107 (1963).
24. A. M. Morsy, M. T. Barako, V. Jankovic, V. D. Wheeler, M. W. Knight, G. T. Papadakis, L. A. Sweatlock, P. W. C. Hon, and M. L. Povinelli, "Experimental demonstration of dynamic thermal regulation using vanadium dioxide thin films," *Scientific Reports* 2020 10:1 10(1), 1–10 (2020).
25. D. Lee, D. Yang, H. Kim, J. Kim, S. Song, K. S. Choi, J. S. Bae, J. Lee, J. Lee, Y. Lee, J. Yan, J. Kim, and S. Park, "Deposition-Temperature-Mediated Selective Phase Transition Mechanism of VO_2 Films," *Journal of Physical Chemistry C* 124(31), 17282–17289 (2020).
26. X. Guo, Y. Tan, Y. Hu, Z. Zafar, J. Liu, and J. Zou, "High quality VO_2 thin films synthesized from V_2O_5 powder for sensitive near-infrared detection," *Scientific Reports* 2021 11:1 11(1), 1–9 (2021).
27. L. Piñol, K. Rebello, K. Caruso, A. S. Francomacaro, and G. L. Coles, "Physical vapor deposition and patterning of calcium fluoride films," *Journal of Vacuum Science & Technology A: Vacuum, Surfaces, and Films* 29(2), 021001 (2011).
28. "See Supplemental Material for details on the transient FEM simulations and an analysis of the effect of reducing the number of layers"
29. D. M. Pozar, *Microwave Engineering*, 4th Edition (2011).
30. Y. Li, Y. Ren, Y. Bai, M. Ikram, Y. Xu, Y. Wang, and Z. Zhang, "Double-Layer Chiral System with Induced Circular Dichroism by Near-Field Coupling," *The Journal of Physical Chemistry C* 125(46), 25851–25858 (2021).
31. S. Bonora, U. Bortolozzo, S. Residori, R. Balu, and P. v. Ashrit, "Mid-IR to near-IR image conversion by thermally induced optical switching in vanadium dioxide," *Optics Letters*, Vol. 35, Issue 2, pp. 103–105 35(2), 103–105 (2010).
32. T. Ben-Messaoud, G. Landry, J. P. Gariépy, B. Ramamoorthy, P. v. Ashrit, and A. Haché, "High contrast optical switching in vanadium dioxide thin films," *Opt Commun* 281(24), 6024–6027 (2008).
33. M. F. Jager, C. Ott, P. M. Kraus, C. J. Kaplan, W. Pouse, R. E. Marvel, R. F. Haglund, D. M. Neumark, and S. R. Leone, "Tracking the insulator-to-metal phase transition in VO_2 with few-femtosecond extreme UV transient absorption spectroscopy," *Proc Natl Acad Sci U S A* 114(36), 9558–9563 (2017).
34. A. Cavalleri, C. Tóth, C. W. Siders, J. A. Squier, F. Ráksi, P. Forget, and J. C. Kieffer, "Femtosecond Structural Dynamics in VO_2 during an Ultrafast Solid-Solid Phase Transition," *Phys Rev Lett* 87(23), 237401 (2001).
35. M. F. Becker, A. B. Buckman, R. M. Walser, T. Lépine, P. Georges, and A. Brun, "Femtosecond laser excitation of the semiconductor-metal phase transition in VO_2 ," *Appl Phys Lett* 65(12), 1507 (1998).
36. A. Butler and C. Argyropoulos, "Mechanically tunable radiative cooling for adaptive thermal control," *Appl Therm Eng* 211, 118527 (2022).

Supplementary Material

Tunable Directional Filter for Mid-Infrared Optical Transmission Switching

Andrew Butler, Jack Schulz, and Christos Argyropoulos*

Department of Electrical and Computer Engineering, University of Nebraska-Lincoln, Lincoln, Nebraska 68588, USA

[*christos.argyropoulos@unl.edu](mailto:christos.argyropoulos@unl.edu)

Transient simulation details

The Finite Element Method (FEM) full wave simulation software Comsol Multiphysics® was used to analyze the transient behavior of the presented vanadium dioxide (VO_2) directional filter. Figure S1 shows a schematic of the electromagnetic simulation set-up. Port boundary conditions were used to launch either transverse magnetic (TM) or transverse electric (TE) polarized plane waves. The side boundaries were simulated using periodic boundary conditions. The VO_2 and calcium fluoride (CaF_2) materials were modelled using their frequency dielectric constants [1,2].

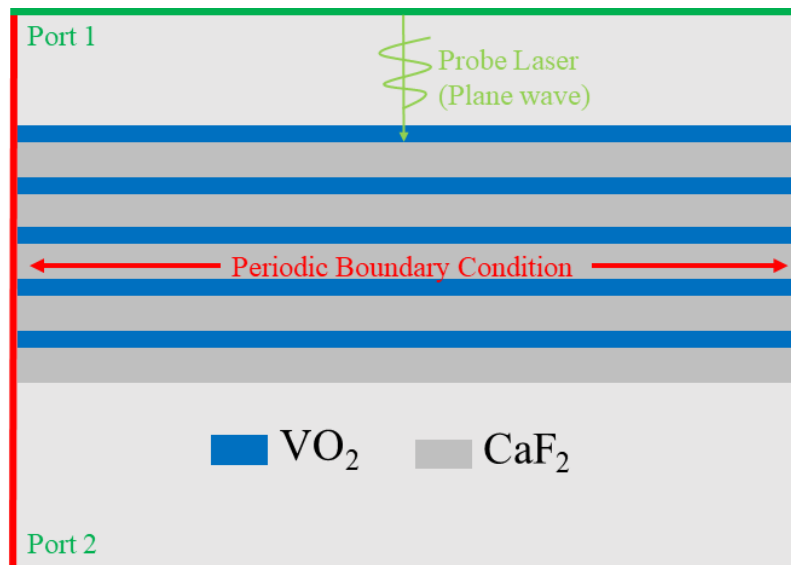


Fig S1. Schematic of the electromagnetic simulation and boundary conditions.

A pump-probe laser setup was used to model the transient heating process and calculate the transmittance as a function of time. Both pump and probe lasers were launched from the port 1 boundary. The probe laser wavelength and input intensity were selected to resemble realistic laser parameters. Two lasers were used as probes in the modeling, where the first is a Thulium (Tm) doped fiber continuous wave (CW) laser operating at 1940nm and the second is a yttrium vanadate (Nd:YVO₄) CW laser emitting at 532nm. The input power intensity was varied between 2.5-10mW/cm². Typical lasers have a Gaussian beam spatial profile, but the small area of the simulation geometry allowed us to approximate the laser as a plane wave. The probe CW lasers were chopped at 5ms duration to demonstrate the effect of VO₂ phase transition in the transmittance of the filter.

The temperature of the filter was initialized to room temperature (293K) and was set uniform throughout the structure at this initial point. The COMSOL's electromagnetic heating interface was used to introduce a heat source term to the heat interface according to the following equations:

$$Q_e = Q_{rh} + Q_{ml}, \quad (1)$$

$$Q_{rh} = \frac{1}{2} \text{Re}(\mathbf{J} \cdot \mathbf{E}^*), \quad (2)$$

$$Q_{ml} = \frac{1}{2} \text{Re}(i\omega \mathbf{B} \cdot \mathbf{H}^*), \quad (3)$$

where Q_e is the total heat added to the system from electromagnetic heating, Q_{rh} is the heat from resistive losses, Q_{ml} is the heat from magnetic losses, \mathbf{J} is the current density, \mathbf{E} is the induced electric field, ω is the angular frequency, and \mathbf{B} and \mathbf{H} are the induced magnetic flux density and field, respectively. Since the materials at the currently studied frequency range are nonmagnetic, Eq. (3) can be neglected, and heating occurs entirely due to the electric field. A schematic of the heating simulation is shown in Fig. S2. Periodic conditions are imposed on the side boundaries of the model, and an ambient temperature of 293K (room temperature) is applied to the top and bottom boundaries. VO₂ and CaF₂ are modelled in the thermal simulations using their thermal conductivity, heat capacity, and density values taken from experimental data [4,5].

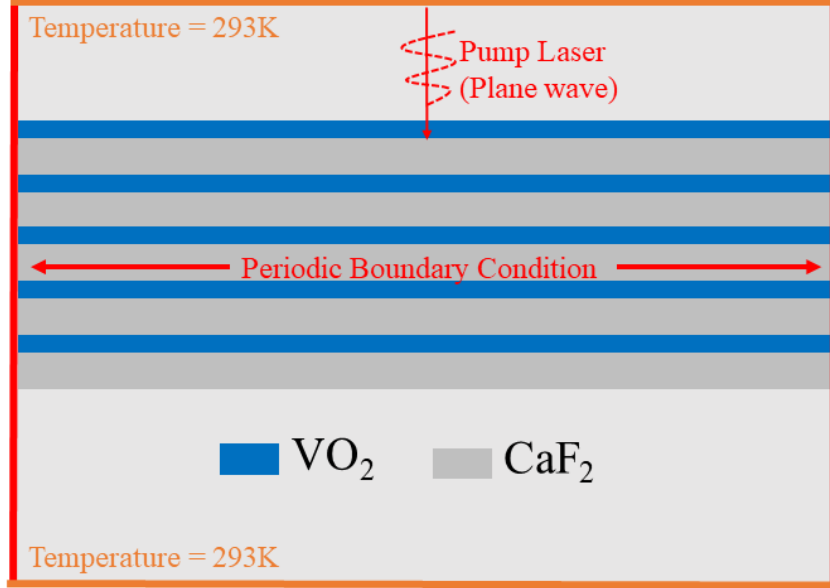


Fig. S2 Schematic of the thermal simulation and boundary conditions.

Once the temperature of the structure was determined, the VO₂ dielectric constant was calculated using Eqs. (4)-(5) in the main paper and the pump laser was launched from the port boundary. The pump laser was modelled as a TM polarized plane wave with 7.6 μ m wavelength but similar response is obtained for TE polarization, as depicted in Fig. 1d in the main paper. The S-parameter calculations were performed to calculate the reflection and transmission coefficients of the structure and the port boundaries measured the total reflected and transmitted power flow through the structure. The power flow through each port was calculated using:

$$P = \int_C \vec{S} \cdot \vec{n} = \frac{1}{2} \int_C \text{Re}\{\vec{E} \times \vec{H}^*\} \cdot \vec{n}, \quad (4)$$

where \vec{S} is the time averaged Poynting Vector, C is the curve of the port boundary, \vec{n} is the normal vector, \vec{E} is the electric field vector, and \vec{H} is the magnetic field vector. The S-parameters were then calculated as:

$$S_{11} = \sqrt{\frac{\text{power reflected back to port 1}}{\text{power emitted from port 1}}}, \quad (5)$$

$$S_{21} = \sqrt{\frac{\text{power transmitted to port 2}}{\text{power emitted from port 1}}}. \quad (6)$$

The reflectance and transmittance were finally computed as $R = |S_{11}|^2$ and $T = |S_{21}|^2$, respectively.

Effect of number of layers

The effect of reducing the number of unit cells or layers in the filter is demonstrated in Fig. S3. Figures S3a, S3b, and S3c demonstrate the transmittance as a function of angle for 3, 4, and 5 unit cells, where each unit cell is composed of one layer of VO₂ and one layer of CaF₂. The spectral transmittance comparison of the same filter for 3, 4, and 5 unit cells is demonstrated in Fig S3d for the normal incidence case. Finally, the angular transmittance of the filter for 3, 4, and 5 unit cells is shown in Fig. S3e. Decreasing the number of unit cells widens the transmission bandwidth of the filter, reduces directionality, and slightly increases transmittance. The effect on the filter performance is not drastic, however for some applications reducing the number of unit cells could help reduce cost and simplify fabrication.

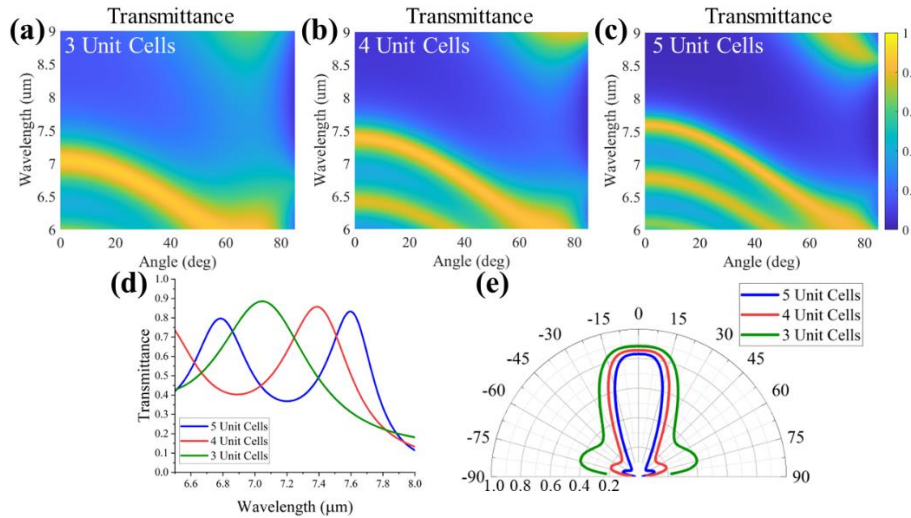


Fig. S3: Transmittance as a function of wavelength and incident angle for (a) 3, (b) 4, and (c) 5 unit cells, respectively. (d) Transmittance spectrum for 3, 4, and 5 unit cells at normal incidence illumination. (e) Directional transmittance pattern as a function of angle for 3, 4, and 5 unit cells. The wavelengths used in this plot are selected to coincide with each design's maximum transmission point.

Figure S4 shows the transient simulation results for 3 unit cells compared to the 5 unit cell case which is presented in Fig. 4 in the main paper. More specifically, Figs. S4a and S4b depict the temperature as a function of time while Figs. S4c and S4d demonstrate the transmittance as a function of time for the simulated yttrium vanadate (Nd:YVO₄) and Thulium (Tm) doped fiber probe lasers. Pump laser intensities of 7.5mW/cm² and 10mW/cm² are used for these simulations for both yttrium vanadate and Tm doped fiber lasers, respectively. Reducing the number of unit cells decreases the phase switching times in the case of the yttrium vanadate laser. The insulator-metal transition time is reduced from 186μs to 139μs and the metal-insulator transition time is reduced from 335μs to 56μs. This is because there is less material to be heated and the heat diffuses throughout the entire filter more quickly. However, for the case of the Tm doped fiber laser, the insulator-metal transition time is increased from 361μs to 661μs and the metal-insulator transition time is reduced from 368μs to 152μs. This is due to the weaker absorption of insulating VO₂ at the Tm doped laser's wavelength. Reducing the number of VO₂ layers decreases the overall filter absorption which, subsequently, slows the heating process. On the other hand, reducing the size of the filter enables faster cooling, which decreases the metal-insulator transition time. Once the VO₂ becomes metallic, the temperature increases quickly because the absorption is always higher in the metallic phase. Finally, the choice of probe laser is important for the heating process due to the distinct wavelength emitted from each probe laser that will interact in a different way with the geometrical features of each layer along the filter structure.

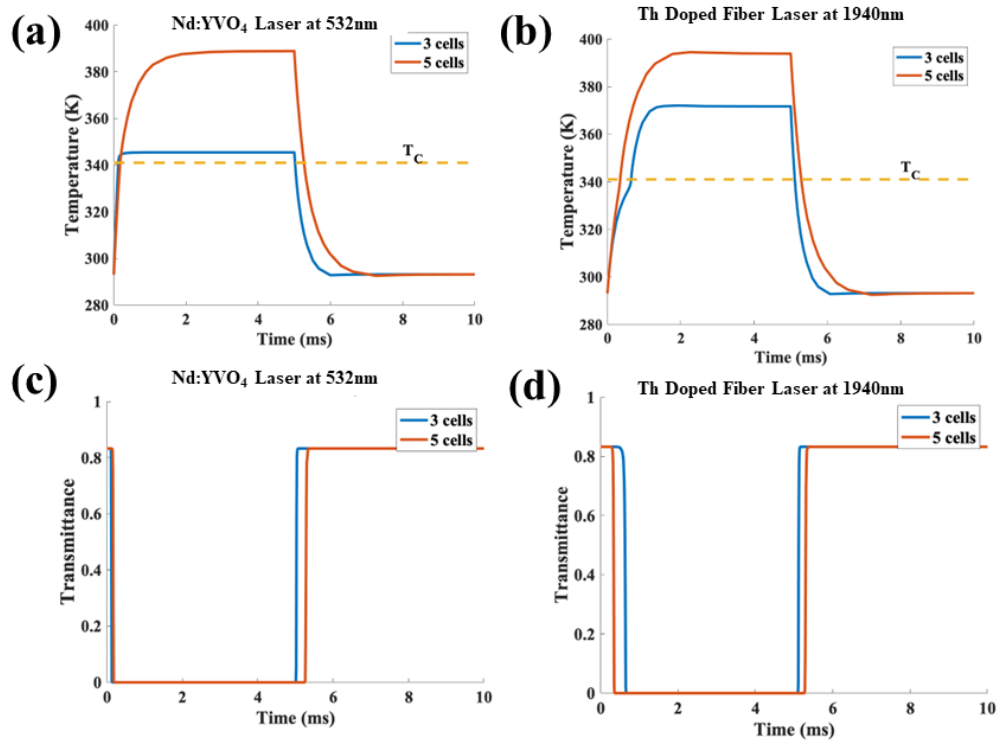


Fig. S4: (a)-(b) Temperature and (c)-(d) transmittance of the directional filter with 3 and 5 unit cells as a function of time for the (a), (c) Nd:YVO₄ and (b), (d) Th doped fiber pump laser when illuminated by fixed intensities of 7.5mW/cm² and 10mW/cm², respectively.

Reflection and absorption in the metallic state

In the metallic state, the transmittance of the filter drops to zero and the reflectance and absorptance are increased. Figure S5 shows the absorptance and reflectance of the filter as a function of angle and wavelength for VO₂ in the metallic state. At angles near normal incidence, the filter exhibits mirror-like response with some absorption, while for higher angles of incidence the device becomes a broadband absorber. This defines two extra functionalities of the proposed filter design as a reflector and a directional broadband absorber.

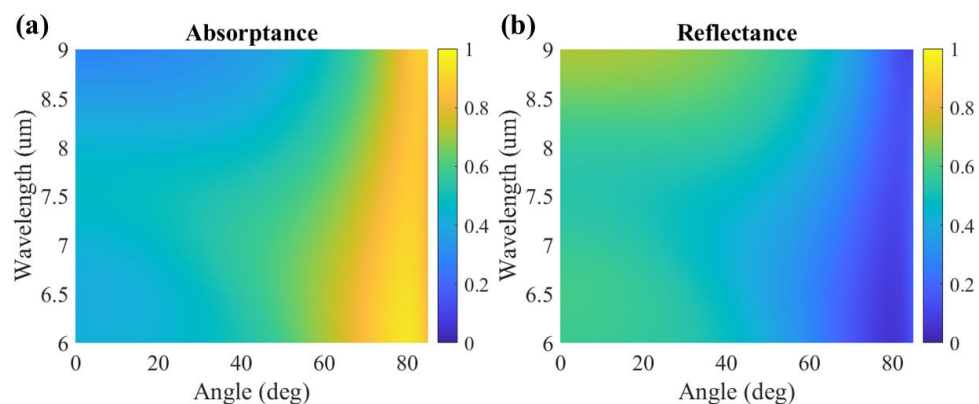


Fig. S5. (a) Absorptance and (b) reflectance as a function of incident angle and wavelength for the filter when VO_2 is in the metallic state.

References

1. A. M. Morsy, M. T. Barako, V. Jankovic, V. D. Wheeler, M. W. Knight, G. T. Papadakis, L. A. Sweatlock, P. W. C. Hon, and M. L. Povinelli, "Experimental demonstration of dynamic thermal regulation using vanadium dioxide thin films," *Scientific Reports* 2020 10:1 **10**(1), 1–10 (2020).
2. H. H. Moore, "Refractive index of alkaline earth halides and its wavelength and temperature derivatives," *Journal of Physical and Chemical Reference Data* **9**(1), 161 (2009).
3. Y. Li, Y. Ren, Y. Bai, M. Ikram, Y. Xu, Y. Wang, and Z. Zhang, "Double-Layer Chiral System with Induced Circular Dichroism by Near-Field Coupling," *The Journal of Physical Chemistry C* **125**(46), 25851–25858 (2021).
4. *The Crystran Handbook of Infra-Red and Ultra-Violet Optical Materials*, 2021 Edition (Crystran Ltd, 2021).
5. G. Hamaoui, N. Horny, C. L. Gomez-Heredia, J. A. Ramirez-Rincon, J. Ordonez-Miranda, C. Champeaux, F. Dumas-Bouchiat, J. J. Alvarado-Gil, Y. Ezzahri, K. Joulain, and M. Chirtoc, "Thermophysical characterisation of VO_2 thin films hysteresis and its application in thermal rectification," *Scientific Reports* 2019 9:1 **9**(1), 1–10 (2019).